Exploring the Role of the "Ice-Ocean Governor" and Mesoscale Eddies in the Equilibration of the Beaufort Gyre: Lessons from Observations®

GIANLUCA MENEGHELLO, EDWARD DODDRIDGE, JOHN MARSHALL, JEFFERY SCOTT, AND JEAN-MICHEL CAMPIN

Department of Earth, Atmospheric and Planetary Sciences, Massachusetts Institute of Technology, Cambridge, Massachusetts

(Manuscript received 26 October 2018, in final form 1 October 2019)

ABSTRACT

Observations of Ekman pumping, sea surface height anomaly, and isohaline depth anomaly over the Beaufort Gyre are used to explore the relative importance and role of (i) feedbacks between ice and ocean currents, dubbed the "ice—ocean governor," and (ii) mesoscale eddy processes in the equilibration of the Beaufort Gyre. A two-layer model of the gyre is fit to observations and used to explore the mechanisms governing the gyre evolution from the monthly to the decennial time scale. The ice—ocean governor dominates the response on interannual time scales, with eddy processes becoming evident only on the longest, decadal time scales.

1. Introduction

The Arctic Ocean's Beaufort Gyre, centered in the Canada basin, is a large-scale, wind-driven, anticyclonic circulation pattern characterized by a strong halocline stratification with relatively fresh surface waters overlying saltier (and warmer) waters of Atlantic Ocean origin. The halocline stratification inhibits the vertical flux of ocean heat to the overlying sea ice cover. Ekman pumping associated with a persistent but highly variable Arctic high pressure system (Proshutinsky and Johnson 1997; Proshutinsky et al. 2009, 2015; Giles et al. 2012) accumulates freshwater and inflates isopycnals. The induced isopycnal slope drives a geostrophically balanced flow whose imprint can be clearly seen in the doming of sea surface height at the center of the Beaufort Sea (see Fig. 1).

Recent observational studies by Meneghello et al. (2017, 2018b), Dewey et al. (2018), and Zhong et al. (2018) have outlined how the interaction between the ice and the surface current plays a central role in the equilibration of the Beaufort Gyre's geostrophic current

Corresponding author: Gianluca Meneghello, gianluca.meneghello@gmail.com

intensity and its freshwater content. Downwelling-favorable winds and ice motion inflate the gyre until the relative velocity between the geostrophic current and the ice velocity is close to zero, at which point the surface-stress-driven Ekman pumping is turned off, and the gyre inflation is halted. In Meneghello et al. (2018a) we developed a theory describing this negative feedback between the ice drift and the ocean currents. We called it the "ice-ocean governor" by analogy with mechanical governors that regulate the speed of engines and other devices through dynamical feedbacks (Maxwell 1867; Bennet 1993; OED 2018).

Another mechanism at work, studied by Davis et al. (2014), Manucharyan et al. (2016), Manucharyan and Spall (2016), and Meneghello et al. (2017), and mimicking the mechanism of equilibration hypothesized for the Antarctic Circumpolar Current (ACC) by Marshall et al. (2002) and Karsten et al. (2002), relies on eddy fluxes to release freshwater accumulated by the persistent anticyclonic winds blowing over the gyre. In this scenario, representing the case of ice in free drift, or the case of an ice free gyre, the ice—ocean governor does not operate and the gyre inflates until baroclinic instability is strong enough to balance the freshwater input.

In this study, we start from observations and address how both mechanisms interact in a real-world Arctic, where we expect their role to change over the seasonal cycle as ice cover and ice mobility vary. A theory for their combined role in the equilibration of the Beaufort Gyre

DOI: 10.1175/JPO-D-18-0223.1

Supplemental information related to this paper is available at the Journals Online website: https://doi.org/10.1175/JPO-D-18-0223.s1.

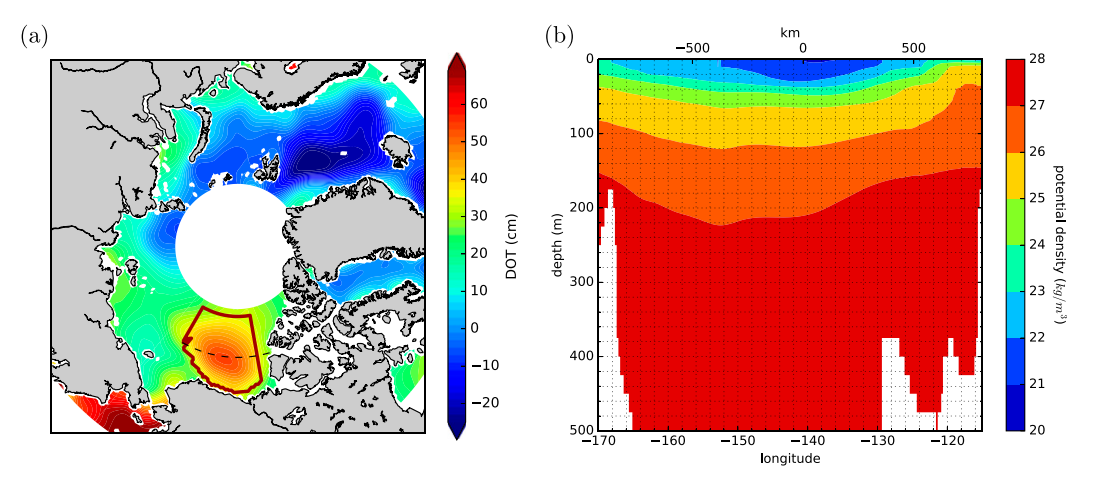


FIG. 1. (a) The doming of satellite-derived dynamic ocean topography (DOT) marks the persistent anticyclonic circulation the Beaufort Gyre, one of the main features of the Arctic Ocean (color; 2003–14 mean; data from Armitage et al. 2016). The white area is beyond the 81.5°N latitudinal limit of the *Envisat* satellite. The Beaufort Gyre region used for computations in this study, including only locations within 70.5°–80.5°N and 170°–130°W whose depth is greater than 300 m, is marked by the thick red line. (b) A section across the Beaufort Gyre region at 75°N, marked by a dashed line in (a), shows how the doming up of the sea surface height toward the middle of the gyre is reflected in the bowing down of isopycnals. The stratification is dominated by salinity variations and concentrated close to the surface, with potential densities ranging from a mean value of 1021 kg m⁻³ at the surface to close to 1028 kg m⁻³ at a depth of about 200 m, and remaining almost constant below that.

has been recently proposed by Doddridge et al. (2019). Here we begin by assimilating time series of Ekman pumping, inferred from observations (see Meneghello et al. 2018b), and sea surface height, obtained from satellite measurements (Armitage et al. 2016, see Fig. 1a) into a two-layer model of the Beaufort Gyre (see Fig. 2). Despite its limitations, as we shall see, our model is able to capture much of the observed variability of the gyre. We then evaluate the relative role of the ice—ocean governor and eddy fluxes in equilibrating the gyre's isopycnal depth anomaly, and its freshwater content. We conclude by using these new insights to discuss how changes in the Arctic ice cover will impact the state of the Beaufort Gyre.

2. Two-layer model of the Beaufort Gyre

Let us consider a two-layer model comprising the sea surface height η and isopycnal depth anomaly a, as shown in Fig. 2 (see section 12.4 of Cushman-Roisin and Beckers 2010). For time scales T longer than one day $[Ro_T=(1/fT)<0.1]$, where $f=1.45\times10^{-4}\,\mathrm{s}^{-1}$ is the Coriolis parameter, and is assumed constant] and length scales L larger than 5 km [Ro=(U/fL)<0.1], where $U\approx 5\,\mathrm{cm}\,\mathrm{s}^{-1}$ is a characteristic velocity], currents in the interior of the Beaufort Gyre can be considered in geostrophic balance everywhere except at the very top and bottom of the water column, where frictional effects drive a divergent Ekman transport. The dynamics of the sea surface height and isopycnal depth anomalies can then be approximated by

$$\frac{d(\eta - a)}{dt} = K \frac{a}{L^2} - \underbrace{\overline{w}_{Ek}}_{top Ekman},$$

$$\frac{da}{dt} = -K \frac{a}{L^2} - \underbrace{\frac{d}{2f} \frac{g\eta + g'a}{L^2}}_{T},$$
(1)

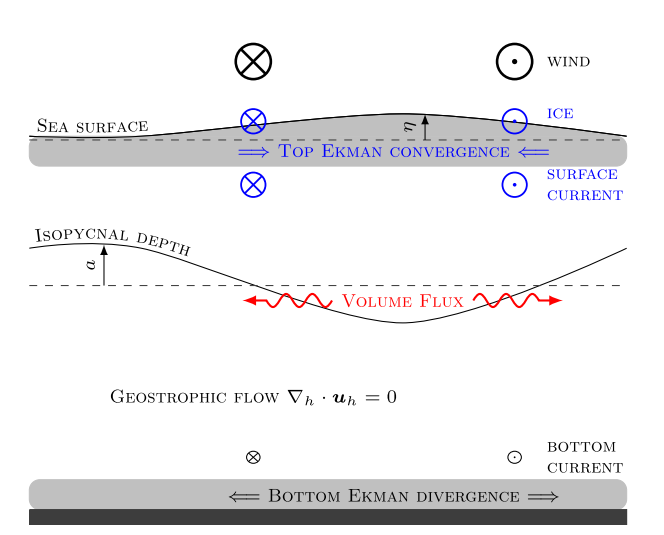


FIG. 2. Schematic of the idealized two-layer model: the wind- and ice-driven Ekman flow (blue) drives variations in the layer thicknesses or, equivalently, in the sea surface height η and isopycnal depth a. The interior is assumed to be in geostrophic balance, and eddy processes (red) result in a volume flux flattening the isopycnal slope.

where $1/L^2$ represents a scaling for the Laplacian operator [see appendix A for a detailed derivation of (1)]. Volume is gathered and released by the surface Ekman pumping $\overline{w}_{\rm Ek} = (1/A) \int_A (\nabla \times \tau/\rho f) \, dA$, proportional to the curl of the surface stress τ , and by the bottom Ekman pumping $-(d/2f)[(g\eta+g'a)/L^2]$, proportional to the Ekman layer length scale d and driven by the bottom geostrophic current $(\hat{k}/f) \times \nabla (g\eta+g'a)$ (see section 8.4 of Cushman-Roisin and Beckers 2010). The term $K(a/L^2)$ represents mesoscale eddies acting to flatten density surfaces. Vertical diffusivity is relatively low in the Arctic and, for simplicity, it is neglected in our model.

The reference water density is taken as $\rho = 1028 \,\mathrm{kg} \,\mathrm{m}^{-3}$, and g and $g' = (\Delta \rho/\rho)g$ are the gravity and reduced gravity constants, with $\Delta \rho$ the difference between the potential density at the surface and at depth.

For the purpose of our discussion we consider the surface stress τ , to have a wind-driven τ_a and an ice-driven τ_i component, weighted by the ice concentration α

$$\boldsymbol{\tau} = (1 - \alpha) \underbrace{\rho_a C_{Da} |\mathbf{u}_a| \mathbf{u}_a}_{\boldsymbol{\tau}_a} + \alpha \underbrace{\rho C_{Di} |\mathbf{u}_i - \mathbf{u}_g| (\mathbf{u}_i - \mathbf{u}_g)}_{\boldsymbol{\tau}_i}, \quad (2)$$

where \mathbf{u}_a , \mathbf{u}_i , and \mathbf{u}_g are the observed wind, ice, and surface geostrophic current velocities, respectively, $\rho_a = 1.25 \,\mathrm{kg} \,\mathrm{m}^{-3}$ is the air density, and $C_{Da} = 0.00125$ and $C_{Di} = 0.0055$ are the air–ocean and ice–ocean drag coefficients. We note how the geostrophic surface currents \mathbf{u}_g act as a negative feedback on the ice-driven component (see Meneghello et al. 2018a).

To better understand the relative role of the winds, sea ice, ocean geostrophic currents, and eddy diffusivity in the equilibration of the gyre, we additionally compute the contribution of the geostrophic current to the ice stress as

$$\boldsymbol{\tau}_{ig} = \boldsymbol{\tau}_i - \boldsymbol{\tau}_{i0}, \tag{3}$$

where τ_{i0} is the ice-ocean stress neglecting the geostrophic current, that is, computed by setting $\mathbf{u}_g = 0$ in (2). Accordingly, we define the Ekman pumping associated with each component as

$$w_a = \frac{\nabla \times [(1 - \alpha) \tau_a]}{\rho f}, \quad w_i = \frac{\nabla \times (\alpha \tau_i)}{\rho f},$$

$$w_{i0} = \frac{\nabla \times (\alpha \boldsymbol{\tau}_{i0})}{\rho f}, \qquad w_{ig} = \frac{\nabla \times (\alpha \boldsymbol{\tau}_{ig})}{\rho f},$$
 (4)

so that the total Ekman pumping can be written as

$$w_{\rm Ek} = w_a + w_i = w_a + w_{i0} + w_{ig}. \tag{5}$$

We also note that the eddy flux term $K(a/L^2)$, having units of meters per year, can be expressed as an equivalent Ekman pumping and compared with the other Ekman velocities.

The dynamics in (1) then describe a "wind-driven" Beaufort Gyre where water masses exchanges are limited to Ekman processes at the top and bottom of the domain, with eddies redistributing volume internally.

An observationally based estimate of the relative importance of the ice-ocean governor contribution w_{ig} and the eddy fluxes contribution $K(a/L^2)$ to the equilibration of the Beaufort Gyre is the main focus of our study.

3. Fitting parameters of the two-layer model using observations of the Beaufort Gyre

To estimate the key parameters, we drive the model (1) using observed Ekman pumping \overline{w}_{Ek} , averaged monthly and over the Beaufort Gyre region (BGR, see Fig. 1), and shown as a black curve in Fig. 3a.

Based on observational evidence (see, e.g., Fig. 1 of Meneghello et al. 2018b), we use $L=300\,\mathrm{km}$ as the characteristic length scale over which derivatives of the ice, wind and geostrophic current velocities should be computed. The monthly resolution of the dataset, and the chosen length scale of interest, results in a temporal Rossby number $\mathrm{Ro}_T \approx 3 \times 10^{-3}$ and a Rossby number $\mathrm{Ro} \approx 1 \times 10^{-3}$: the geostrophic approximation behind the derivation of our model (1) is then verified, and the quasigeostrophic correction is negligible (see also appendix A).

We then vary K, g', and d, as well as the initial conditions of sea surface height and isopycnal depth anomalies, to minimize the departure of the estimated sea surface height anomaly from the observed one, shown as a black curve in Fig. 3b. The data used are described in appendix B. The procedure to estimate the five free parameters using the 144 monthly observational data points is outlined in appendix C.

The estimated sea surface height anomaly (Fig. 3b, blue) closely follows the observed one (black) (RMSE = $0.02 \,\mathrm{m}$, $R^2 = 0.68$) and captures relatively well both the seasonal cycle and the relatively sudden changes in sea surface height and isopycnal depth anomaly that occurred in 2007 and 2012, both associated with changes in the ice extent and atmospheric circulation (McPhee et al. 2009; Simmonds and Rudeva 2012). Red squares mark the observed August–October mean 30-psu isohaline depth anomaly, corresponding to the surface layer depth anomaly, and are not used in the data estimation process.

The estimated parameters, and their standard deviations, are $K = (218 \pm 31) \text{ m}^2 \text{ s}^{-1}$ and $g' = (0.065 \pm 0.007) \text{ m s}^{-2}$

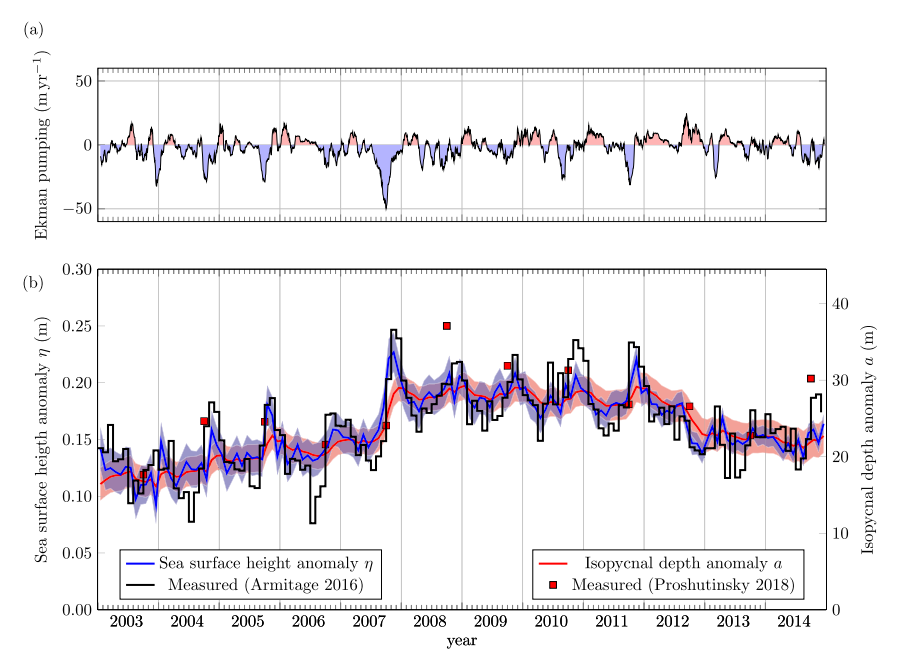


FIG. 3. Observations of monthly (top) mean Ekman pumping (black) and (bottom) mean sea surface height anomaly (black) over the Beaufort Gyre region are assimilated in the idealized model (1). Blue and red filled areas in the top panel denote upwelling and downwelling, respectively. Red marks show the 30-psu isohaline depth anomaly estimated from hydrographic data for August–October of each year (Proshutinsky et al. 2009); in the Arctic, isohaline depth can be considered a good approximation to isopycnal depth because the ocean stratification is mostly due to salinity variations. The estimated sea surface height anomaly (blue), isopycnal depth anomaly (red), eddy diffusivity $K = 218 \,\mathrm{m}^2 \,\mathrm{s}^{-1}$, and reduced gravity $g' = 0.065 \,\mathrm{m} \,\mathrm{s}^{-2}$ (corresponding to $\Delta \rho = 6.8 \,\mathrm{kg} \,\mathrm{m}^{-3}$) are in agreement with observations. In particular, the estimated sea surface height anomaly (blue) captures most of the observed seasonal cycle variability (black) as well as its long-term increase after 2007 (RMSE = $0.02 \,\mathrm{m}$, $R^2 = 0.68$). The estimated bottom Ekman layer thickness is $d = 58 \,\mathrm{m}$, and includes the effects of bottom bathymetry. Shaded blue and red regions in the bottom panel show the uncertainty of the model estimation (one standard deviation).

(or, equivalently, $\Delta \rho = 6.8 \, \mathrm{kg \, m^{-3}}$) broadly in accord with observations [see Meneghello et al. (2017) and Fig. 1b]. The estimated bottom Ekman layer thickness $d = (58 \pm 11)$ m includes bathymetry effects which cannot be represented in our model.

We note that our parameter estimate depends on the choice of the length scale L, so that we will use our estimates primarily to gain a physical intuition of the relative importance of the processes at play. Nonetheless, the fact that such values are very close to observations suggests that the choice of L is appropriate. More importantly, neither the captured variance R^2 —informing us about the accuracy of the model—nor the analysis outlined in the next section depends on the choice of the length scale L.

Our simple model estimates a single constant value of eddy diffusivity for the entire Beaufort Gyre region. Previous work on the Beaufort Gyre has suggested that the eddy diffusivity vary in space (Meneghello et al. 2017) and depends on the state of the large-scale flow

and its history (Manucharyan et al. 2016, 2017), while studies focusing on the Southern Ocean have shown that eddy diffusivity varies in both space and time (Meredith and Hogg 2006; Wang and Stewart 2018). Similarly, in our computation of Ekman pumping (Meneghello et al. 2018b) we assume a constant value for the drag coefficient despite the fact that observational evidence suggests a large variability (Cole et al. 2017). Despite its limitations, our model is able to capture much of the observed variability of the gyre over the time period considered, and will be used in the next section to discuss the relative role of the governor and eddy fluxes in the gyre equilibration.

4. Relative importance of the ice-ocean governor and eddy fluxes

Now that parameters of our model (1) have been estimated using available observations, we can analyze the

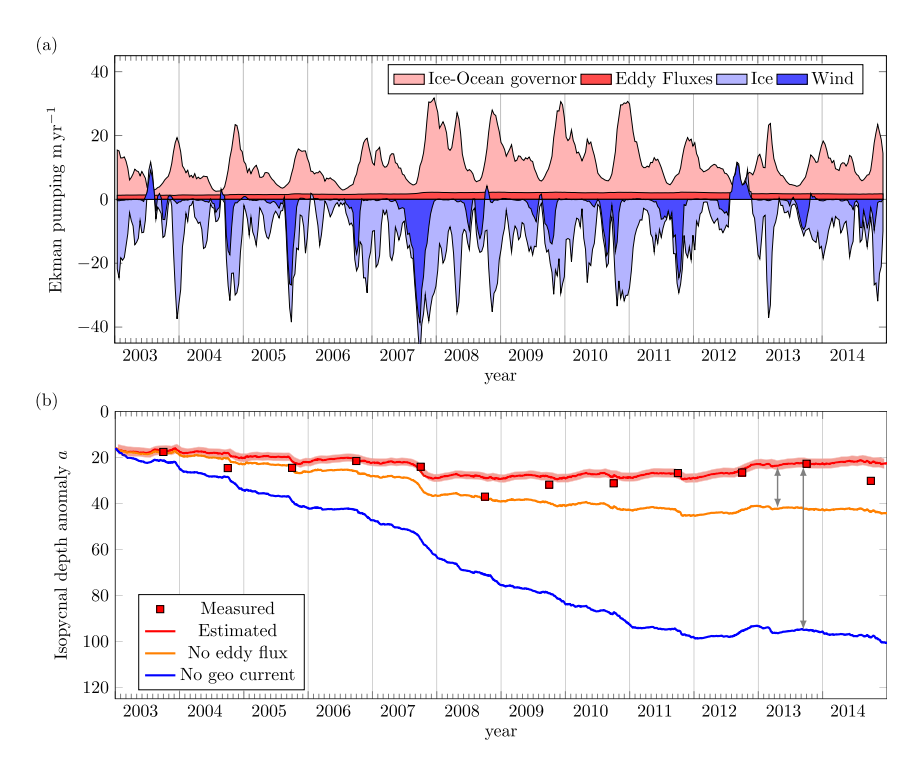


FIG. 4. (a) Ekman pumping associated with wind forcing w_a (dark blue), ice forcing w_{i0} (light blue), eddy fluxes $K(a/L^2)$ (dark red), and the ice-ocean governor w_{ig} (light red). See (4). The mean ice-ocean governor term w_{ig} is 6 times larger than the mean eddy fluxes term Ka/L^2 . (b) Hypothetical isopycnal depth anomaly under different scenarios: red line and red marks are the same as in Fig. 3b, with the red shaded region denoting one standard deviation. The orange curve represents the evolution of the isopycnal obtained by neglecting eddy diffusivity in (1). The blue curve is obtained by neglecting the ice-ocean governor. The error introduced by not including the ice-ocean governor is much larger (gray arrows), with an increase in isopycnal depth anomaly of more than 10 times larger than the actual one over the 12-yr period considered.

different role of each term in the equilibration of the Beaufort Gyre. Figure 4a shows monthly running means of wind-driven w_a and ice-driven w_{i0} downwelling favorable Ekman pumping (cumulative mean of $-12.2 \,\mathrm{m\,yr}^{-1}$, dark and light blue respectively). This is to be compared with the deflating effect of eddy fluxes $K(a/L^2)$ (equivalent to a mean upwelling of 1.8 m yr⁻¹, dark red) and of the upwelling favorable ice-ocean governor Ekman pumping w_{ig} (mean of 9.8 m yr⁻¹ upward, light red). Over the 12 years of the available data, the contribution of the governor, reducing freshwater accumulation by limiting, or at time reversing, Ekman downwelling, is 6 times larger than the freshwater release associated with eddy fluxes. The small residual Ekman pumping of $-0.6 \,\mathrm{m\,yr^{-1}}$ accounts for the 7-m increase in isopycnal depth between 2003 and 2014 (red line in Fig. 3b), consistent with observations.

The ice-ocean governor, acting on both barotropic (fast) and baroclinic (slower) time scales, plays a much

larger role than that of eddy fluxes. As can be seen from Fig. 4, the upwelling effect of the ice-ocean governor (light red) closely mirrors the downwelling effect of the ice motion (light blue), both having important variations over the seasonal cycle, and essentially canceling the net Ekman pumping within the ice covered regions of the gyre. In contrast, eddy fluxes provide a much smaller, but persistent, mechanism releasing the accumulated freshwater and flattening isopycnals.

To gain further insights into the different role played by the two mechanisms in the equilibration of the gyre, we show in Fig. 4b the hypothetical evolution of the isopycnal depth anomaly when neglecting eddy fluxes (orange) and when neglecting the ice-ocean governor (i.e., setting $w_{\rm Ek} = w_a + w_{i0}$), while keeping the eddy diffusivity unchanged at $K = 218\,{\rm m}^2\,{\rm s}^{-1}$ (blue). In both cases, we integrate the gyre model (1) using daily values of Ekman pumping (Meneghello et al. 2018b), starting from the same sea surface height and isopycnal depth anomaly on 1 January 2003. It is clear how the isopycnal

depth anomaly change between 2003 and 2014, estimated in the absence of the ice-ocean governor and with realistic values of eddy diffusivity, would have been more than 10 times the actual value of 7 m, while the error introduced by neglecting the eddy diffusivity would be smaller.

It is of course possible to consider a scenario in which the dominating balance is the one between Ekman pumping and eddy fluxes, as suggested by, for example, Davis et al. (2014) and Manucharyan and Spall (2016). Such scenario can be tested by neglecting the feedback of the geostrophic current w_{ig} from the Ekman pumping [see Eq. (5)] and estimating the eddy fluxes after fixing the stratification to a realistic value of $6.8 \,\mathrm{kg}\,\mathrm{m}^{-3}$. The resulting eddy diffusivity is $(1519 \pm 281) \,\mathrm{m}^2\,\mathrm{s}^{-1}$, while the bottom Ekman layer depth $d = (90 \pm 47) \,\mathrm{m}$. Such value of eddy diffusivity is more typical of the Southern Ocean than the Arctic.

5. Conclusions

Using observational estimates of Ekman pumping (Meneghello et al. 2017) and sea surface height anomaly (Armitage et al. 2016) we have estimated key parameters of a two layer model, and studied the relative effect of eddy fluxes and of the ice-ocean governor on the equilibration of the Beaufort Gyre. Both mechanisms have been previously addressed separately in both theoretical and observational settings by Davis et al. (2014), Manucharyan et al. (2016), Manucharyan and Spall (2016), and Meneghello et al. (2017) and by Meneghello et al. (2018a,b), Dewey et al. (2018), Zhong et al. (2018), and Kwok et al. (2013). A theoretical framework unifying the two has been detailed by Doddridge et al. (2019). Here, however, we have brought the two together in the context of observations, and used those observations to explore the relative importance of the two mechanisms.

In the current state of the Arctic, the ice-ocean governor plays a much more significant role than eddy fluxes in regulating the gyre intensity and its freshwater content. As can be inferred from Fig. 4, this is particularly true on seasonal-to-interannual time scales. We judge that the freshwater not accumulated (by reduced Ekman downwelling) or released (by Ekman upwelling) by the ice-ocean governor is more than 5 times the freshwater released by eddies. This reminds us of how central is the interaction of ice with the underlying ocean in setting the time scale of response of the gyre and its ability to store freshwater. Moreover, this is a very difficult process to capture in models because it demands that we faithfully represent internal lateral stresses within the ice.

Future circulation regimes will be impacted by the changes in the concentration, thickness and mobility of ice that have significantly evolved over the past two decades. In particular, loss of multiyear ice and increased seasonality of the Arctic sea ice extent is to be expected, with summers characterized by ice-free or very mobile ice conditions, and winters characterized by an extensive ice cover (Haine and Martin 2017). Depending on the internal strength of winter ice, the Arctic Ocean could evolve in the following two rather different scenarios. If the ice is very mobile then the present seasonal cycle of upwelling and downwelling (red and blue shaded areas in Fig. 3) would be replaced by persistent, year-long downwelling. This would result in an increase in the depth of the halocline and more accumulation of freshwater. Ultimately the gyre would be stabilized through expulsion of freshwater from the Beaufort Gyre via enhanced eddy activity. However, if winter ice remains rigid, downwelling in the summer will be balanced by upwelling in the winter as the anticyclonic gyre rubs up against the winter-ice cover; stronger geostrophic currents will potentially result in stronger upwelling cycles, affecting the ocean stratification and increasing the variability of the isopycnal depth, geostrophic current and freshwater content over the seasonal cycle. Our ability to predict these changes depends on how well our models can represent the transfer of stress from the wind to the underlying ocean, through the seasonal cycle of ice formation and melting.

Acknowledgments. The authors thankfully acknowledge support from NSF Polar Programs, both Arctic and Antarctic, and the MIT-GISS collaborative agreement.

APPENDIX A

Derivation of the Governing Equations

Let us consider the volume conservation equations for a flat-bottom, two-layer model with layers thicknesses h_1 and h_2 and velocities \mathbf{u}_1 and \mathbf{u}_2 (see section 12.4 of Cushman-Roisin and Beckers 2010)

$$\begin{split} &\frac{\partial h_1}{\partial t} + \nabla \cdot (h_1 \mathbf{u}_1) = 0, \\ &\frac{\partial h_2}{\partial t} + \nabla \cdot (h_2 \mathbf{u}_2) = 0. \end{split} \tag{A1}$$

In the hypothesis of low Rossby Ro = U/fL and temporal Rossby Ro_T = 1/fT numbers, the acceleration and advection terms in the momentum equations can be neglected and the velocity can be decomposed in a

geostrophic $\mathbf{u}_{g1,g2}$ and an Ekman $\mathbf{u}_{e1,e2}$ component, so that for each layer

$$\mathbf{u} = \mathbf{u}_g + \mathbf{u}_e. \tag{A2}$$

The divergence free geostrophic component can be expressed as a function of the layer thicknesses as

$$\begin{split} \mathbf{u}_{g1} &= \frac{g}{f} \hat{\mathbf{k}} \times \nabla (h_1 + h_2), \\ \mathbf{u}_{g2} &= \frac{g}{f} \hat{\mathbf{k}} \times \nabla (h_1 + h_2) + \frac{g'}{f} \hat{\mathbf{k}} \times \nabla h_2, \end{split} \tag{A3}$$

while the vertically integrated volume divergence of the Ekman components, limited to the very top and the very bottom of the two layers (see the gray areas Fig. 2), can be expressed as a function of the surface stress τ and the bottom pressure $p = g(h_1 + h_2) + g'h_2$ as

$$\begin{split} &\nabla \cdot (h_1 \mathbf{u}_{e1}) = -\frac{\nabla \times \boldsymbol{\tau}}{\rho f}, \\ &\nabla \cdot (h_2 \mathbf{u}_{e2}) = -\frac{d}{2\rho f} \nabla^2 [g(h_1 + h_2) + g' h_2]. \end{split} \tag{A4}$$

Using (A4), (A3), and (A2), the volume conservation equation (A1) can be rewritten as

$$\begin{split} \frac{\partial h_1}{\partial t} - \frac{g}{f} (\hat{\mathbf{k}} \times \nabla h_1) \cdot \nabla h_2 - \frac{\nabla \times \boldsymbol{\tau}}{\rho f} &= 0 \,, \\ \frac{\partial h_2}{\partial t} + \frac{g}{f} (\hat{\mathbf{k}} \times \nabla h_1) \cdot \nabla h_2 - \frac{d}{2\rho f} \nabla^2 [g(h_1 + h_2) + g'h_2] &= 0 \,. \end{split} \tag{A5}$$

By defining the mean layer thicknesses H_1 and H_2 , (A5) can be restated in terms of sea surface height anomaly $\eta = h_1 + h_2 - (H_1 + H_2)$ and isopycnal depth anomaly $a = h_2 - H_2$

$$\frac{\partial \eta}{\partial t} + \underbrace{\frac{d}{2\rho f} \nabla^2 (g\eta + g'a)}_{\text{bottom Ekman flux}} - \underbrace{\frac{\nabla \times \tau}{\rho f}}_{\text{top Ekman flux}} = 0,$$

$$\frac{\partial a}{\partial t} + \underbrace{\frac{g}{f}(\hat{\mathbf{k}} \times \nabla \eta) \cdot \nabla a}_{\text{isopycnal advection}} - \underbrace{\frac{d}{2\rho f} \nabla^2 (g\eta + g'a)}_{\text{bottom Ekman flux}} = 0. \quad (A6)$$

We remark that for typical values of $L \approx 100\,\mathrm{km}$, $\eta \approx 0.1\,\mathrm{m}$, $a \approx 10\,\mathrm{m}$, $g' \approx 0.1\,\mathrm{m}^{-2}$, $d \approx 10\,\mathrm{m}$ and for a time scale on the order of a month, all terms are of order 10^{-5} . The only exception is the term $\partial \eta/\partial t$, which, while negligible, is retained to avoid having to deal with an integro-differential equation to assimilate the sea surface height η .

Using an eddy closure for the isopycnal advection term, we can write

$$\frac{g}{f}(\hat{\mathbf{k}} \times \nabla \eta') \cdot \nabla a' = -K\nabla^2 a, \tag{A7}$$

where K is a diffusivity coefficient, η' and a' are perturbations and the mean $(\hat{\mathbf{k}} \times \nabla \overline{\eta}) \cdot \nabla \overline{a}$ is neglected because, on long time scales, the sea surface height and isopycnal depth anomaly gradients are parallel.

Substitution of (A7) in (A6), and the approximation $\nabla^2 = 1/L^2$, gives (1).

APPENDIX B

Data

To constrain the model (1), we use observational estimates of Ekman pumping \overline{w}_{Ek} and sea surface height anomaly η (see the online supplemental material).

Ekman pumping is shown in Fig. 3a, where blue and red shading denote downwelling and upwelling time periods, respectively. We remark how the presence of winter upwelling is a direct consequence of the inclusion of the geostrophic current in our estimates, is in agreement with results from Dewey et al. (2018) and Zhong et al. (2018), and lower than previous estimates by Yang (2006, 2009). The monthly time series of Ekman pumping used in this work is obtained by averaging our Arctic-wide observational estimates (Meneghello et al. 2017, 2018b) over the Beaufort Gyre region (BGR, see Fig. 1), and are thus based on sea ice concentration α from Nimbus-7 SMMR and DMSP SSM/I-SSMIS passive microwave data, version 1 (Cavalieri et al. 1996), sea ice velocity \mathbf{u}_i from the Polar Pathfinder daily 25-km Equal-Area Scalable Earth Grid (EASE-Grid) sea ice motion vectors, version 3 (Tschudi et al. 2016), geostrophic currents \mathbf{u}_{ϱ} computed from dynamic ocean topography (Armitage et al. 2016, 2017), and 10-m wind \mathbf{u}_a from the NCEP-NCAR Reanalysis 1 (Kalnay et al. 1996).

The mean sea surface height anomaly, shown by a black line in Fig. 3b, is computed as the norm of the gradient of sea surface height estimates by Armitage et al. (2016), multiplied by $L=300\,\mathrm{km}$, a characteristic length scale for the wind and ice velocity gradients—see, e.g., Fig. 1 of Meneghello et al. (2018b). The original sea surface height estimate is available on a $0.75^\circ \times 0.25^\circ$ grid, and is obtained by combining *Envisat* (2003–11) and *CryoSat-2* (2012–14) observations of sea surface height from the open ocean and ice-covered ocean (via leads). A total of 1761 grid points from the original dataset are used to compute the BGR-averaged sea surface height anomaly for each month.

While not used to constrain the model, an estimate of the mean isohaline depth anomaly, shown as red marks in Fig. 3b, is obtained in a similar fashion. We start from the 50-km resolution August–October 30-psu isohaline depth estimated using CTD, XCTD, and underway CTD (UCTD) profiles collected each year from July through October, and available at http://www.whoi.edu/page.do?pid=161756. The norm of the isohaline gradient is averaged over the BGR and multiplied by the reference length $L=300\,\mathrm{km}$. A total of 409 grid points are used to compute the BGR-averaged isohaline depth anomaly for each month.

APPENDIX C

Parameter Estimation

In this section we report the MATLAB code for the parameter estimation. The file named "Table A1" (table A1.dat) is provided in the online supplemental material.

```
% load Ekman pumping (we) and
% sea surface height (eta)
% from table A1
infile = readtable('tableA1.dat');
      = infile.wemonthly;
we
eta
      = infile.eta;
% time step is 1 month
     = 3600 \times 24 \times 365/12.;
% initialize Matlab data object
      = iddata(eta, we, dt)
% initialize estimation options
                   = greyestOptions;
greyopt
                   = 'simulation';
greyopt.Focus
% initialize Linear ODE model
% with identifiable parameters
           : eddy diffusivity
%-K
%-d
           : bottom Ekman layer depth
%-drho
            : potential density anomaly
        = { 'K', 300; 'd', 100; 'drho', 6};
sysinit = idgrey('model',pars,'c');
% estimate parameters
[sys,x0] = greyest(z,sysinit,greyopt);
% the linear ODE model (see equation 1)
function [A,B,C,D] = model(K,d,drho,Ts)
rho = 1028.;
                     % reference density
  = 1.45e-4;
                     % Coriolis parameter
   = 9.81;
                     % gravity constant
```

```
gp = g*drho/rho; % reduced gravity
L = 300000.; % reference radius
c1 = d/(2*f)/L²;

A = [ -c1*g, c1*gp;
+c1*g, -c1*gp - K/L^2];
B = [ -1; 0];
C = [ 1, 0];
D = [ 0 ];
end
```

REFERENCES

Armitage, T. W. K., S. Bacon, A. L. Ridout, S. F. Thomas, Y. Aksenov, and D. J. Wingham, 2016: Arctic sea surface height variability and change from satellite radar altimetry and GRACE, 2003–2014. J. Geophys. Res. Oceans, 121, 4303–4322, https://doi.org/10.1002/2015JC011579.

—, —, A. A. Petty, S. Wolbach, and M. Tsamados, 2017: Arctic Ocean geostrophic circulation 2003–2014. *Cryosphere*, 11, 1767–1780, https://doi.org/10.5194/tc-11-1767-2017.

Bennet, S., 1993: A History of Control Engineering, 1930-1955. IET, 262 pp., https://doi.org/10.1049/PBCE047E.

Cavalieri, D. J., C. L. Parkinson, P. Gloersen, and H. J. Zwally, 1996: Sea ice concentrations from Nimbus-7 SMMR and DMSP SSM/I-SSMIS passive microwave data, version 1. NASA National Snow and Ice Data Center Distributed Active Archive Center, accessed 17 May 2018, https://doi.org/ 10.5067/8GO8LZOVL0VL.

Cole, S. T., and Coauthors, 2017: Ice and ocean velocity in the Arctic marginal ice zone: Ice roughness and momentum transfer. *Elem. Sci. Anth.*, **5**, 55, https://doi.org/10.1525/ELEMENTA.241.

Cushman-Roisin, B., and J.-M. Beckers, 2010: *Introduction to Geophysical Fluid Dynamics. Physical and Numerical Aspects*. International Geophysics Series, Vol. 101, Academic Press, 786 pp., https://doi.org/10.1016/B978-0-12-088759-0.00022-5.

Davis, P., C. Lique, and H. L. Johnson, 2014: On the link between arctic sea ice decline and the freshwater content of the Beaufort Gyre: Insights from a simple process model. *J. Climate*, 27, 8170–8184, https://doi.org/10.1175/JCLI-D-14-00090.1.

Dewey, S., J. Morison, R. Kwok, S. Dickinson, D. Morison, and R. Andersen, 2018: Arctic ice-ocean coupling and gyre equilibration observed with remote sensing. *Geophys. Res. Lett.*, 45, 1499–1508, https://doi.org/10.1002/2017GL076229.

Doddridge, E. W., G. Meneghello, J. Marshall, J. Scott, and C. Lique, 2019: A three-way balance in the Beaufort Gyre: The ice-ocean governor, wind stress, and eddy diffusivity. J. Geophys. Res. Oceans, 124, 3107–3124, https://doi.org/ 10.1029/2018JC014897.

Giles, K. A., S. W. Laxon, A. L. Ridout, D. J. Wingham, and S. Bacon, 2012: Western Arctic Ocean freshwater storage increased by wind-driven spin-up of the Beaufort Gyre. *Nat. Geosci.*, **5**, 194–197, https://doi.org/10.1038/ngeo1379.

Haine, T. W., and T. Martin, 2017: The Arctic-Subarctic sea ice system is entering a seasonal regime: Implications for future Arctic amplification. Sci. Rep., 7, 4618, https://doi.org/10.1038/ s41598-017-04573-0.

Kalnay, E., and Coauthors, 1996: The NCEP/NCAR 40-Year Reanalysis Project. Bull. Amer. Meteor. Soc., 77, 437–471, https://doi.org/10.1175/1520-0477(1996)077<0437:TNYRP>2.0.CO;2.

- Karsten, R., H. Jones, and J. Marshall, 2002: The role of eddy transfer in setting the stratification and transport of a circumpolar current. J. Phys. Oceanogr., 32, 39–54, https://doi.org/ 10.1175/1520-0485(2002)032<0039:TROETI>2.0.CO;2.
- Kwok, R., G. Spreen, and S. Pang, 2013: Arctic sea ice circulation and drift speed: Decadal trends and ocean currents. J. Geophys. Res. Oceans, 118, 2408–2425, https://doi.org/10.1002/jgrc.20191.
- Manucharyan, G. E., and M. A. Spall, 2016: Wind-driven fresh-water buildup and release in the Beaufort Gyre constrained by mesoscale eddies. *Geophys. Res. Lett.*, 43, 273–282, https://doi.org/10.1002/2015GL065957.
- ——, and A. F. Thompson, 2016: A theory of the wind-driven Beaufort Gyre variability. J. Phys. Oceanogr., 46, 3263–3278, https://doi.org/10.1175/JPO-D-16-0091.1.
- —, A. F. Thompson, and M. A. Spall, 2017: Eddy memory mode of multidecadal variability in residual-mean ocean circulations with application to the Beaufort Gyre. *J. Phys. Oceanogr.*, 47, 855–866, https://doi.org/10.1175/JPO-D-16-0194.1.
- Marshall, J., H. Jones, R. Karsten, and R. Wardle, 2002: Can eddies set ocean stratification? *J. Phys. Oceanogr.*, **32**, 26–38, https://doi.org/10.1175/1520-0485(2002)032<0026:CESOS>2.0 CO²2.
- Maxwell, J. C., 1867: On governors. Proc. Roy. Soc. London, 16, 270–283, https://doi.org/10.1098/RSPL.1867.0055.
- McPhee, M. G., A. Proshutinsky, J. H. Morison, M. Steele, and M. B. Alkire, 2009: Rapid change in freshwater content of the Arctic Ocean. *Geophys. Res. Lett.*, 36, L10602, https://doi.org/ 10.1029/2009GL037525.
- Meneghello, G., J. Marshall, S. T. Cole, and M.-L. Timmermans, 2017: Observational inferences of lateral eddy diffusivity in the halocline of the Beaufort Gyre. *Geophys. Res. Lett.*, 44, 12 331–12 338, https://doi.org/10.1002/2017GL075126.
- —, —, J.-M. Campin, E. Doddridge, and M.-L. Timmermans, 2018a: The ice-ocean governor: Ice-ocean stress feedback limits Beaufort Gyre spin-up. *Geophys. Res. Lett.*, 45, 11293– 11299, https://doi.org/10.1029/2018GL080171.
- —, —, M.-L. Timmermans, and J. Scott, 2018b: Observations of seasonal upwelling and downwelling in the Beaufort Sea

- mediated by sea ice. *J. Phys. Oceanogr.*, **48**, 795–805, https://doi.org/10.1175/JPO-D-17-0188.1.
- Meredith, M. P., and A. M. Hogg, 2006: Circumpolar response of Southern Ocean eddy activity to a change in the Southern Annular Mode. *Geophys. Res. Lett.*, **33**, L16608, https://doi.org/10.1029/2006GL026499.
- OED, 2018: Governor. Oxford English Dictionary, Oxford University Press.
- Proshutinsky, A., and M. A. Johnson, 1997: Two circulation regimes of the wind-driven Arctic Ocean. *J. Geophys. Res.*, 102, 12 493–12 514, https://doi.org/10.1029/97JC00738.
- —, and Coauthors, 2009: Beaufort Gyre freshwater reservoir: State and variability from observations. J. Geophys. Res., 114, C00A10, https://doi.org/10.1029/2008JC005104.
- —, D. Dukhovskoy, M.-l. Timmermans, R. Krishfield, and J. L. Bamber, 2015: Arctic circulation regimes. *Philos. Trans. Roy. Soc. London*, 373A, 20140160, https://doi.org/10.1098/RSTA.2014.0160.
- Simmonds, I., and I. Rudeva, 2012: The great Arctic cyclone of August 2012. Geophys. Res. Lett., 39, L23709, https://doi.org/ 10.1029/2012GL054259.
- Tschudi, M., C. Fowler, J. S. Maslanik, and W. Meier, 2016: Polar Pathfinder daily 25 km EASE-Grid sea ice motion vectors, version 3. NSIDC, accessed 17 May 2018, https://doi.org/10.5067/O57VAIT2AYYY.
- Wang, Y., and A. L. Stewart, 2018: Eddy dynamics over continental slopes under retrograde winds: Insights from a model intercomparison. *Ocean Modell.*, 121, 1–18, https://doi.org/10.1016/ j.ocemod.2017.11.006.
- Yang, J., 2006: The seasonal variability of the Arctic Ocean Ekman transport and its role in the mixed layer heat and salt fluxes. J. Climate, 19, 5366–5387, https://doi.org/10.1175/JCLI3892.1.
- ——, 2009: Seasonal and interannual variability of downwelling in the Beaufort Sea. J. Geophys. Res., 114, C00A14, https:// doi.org/10.1029/2008JC005084.
- Zhong, W., M. Steele, J. Zhang, and J. Zhao, 2018: Greater role of geostrophic currents in ekman dynamics in the western Arctic Ocean as a mechanism for Beaufort Gyre stabilization. *J. Geophys. Res. Oceans*, 123, 149–165, https://doi.org/10.1002/ 2017JC013282.